ACS APPLIED ENERGY MATERIALS

www.acsaem.org

Article

In Situ X-ray Diffraction of $LiCoO_2$ in Thin-Film Batteries under High-Voltage Charging

Tsuyoshi Ohnishi, Kazutaka Mitsuishi, and Kazunori Takada*

Cite This: *ACS Appl. Energy Mater.* 2021, 4, 14372−14379

Read Online

ACCESS | Metrics & More | Article Recommendations

ABSTRACT: $LiCoO_2$ has been used as the cathode material employed in lithium-ion batteries since their development, and efforts to improve its performance are still in progress. For example, complete use of lithium provides a theoretical capacity as high as 274 mAh g^{-1}; however, charge−discharge cycling with such a high capacity leads to rapid degradation. The degradation mechanism has been intensively studied in order to increase the practical capacity. Although phase transitions taking place in high-voltage charging have been considered to affect the cycling performance, side reactions induced by the high-voltage charging always overlap to blur the effects of phase transitions on the electrode properties. This study has unveiled the relation between the phase transition and electrode properties by employing a solid electrolyte that suppresses the side reactions efficiently. Electrochemical impedance spectroscopy combined with in situ X-ray diffraction shows clear correlation between phase transition from O3 to H1−3 and a drastic increase in the electrode resistance. The increasing resistance is attributable to formation of narrow interlayers with a gallery height of 4.2 Å that impede lithium-ion diffusion.

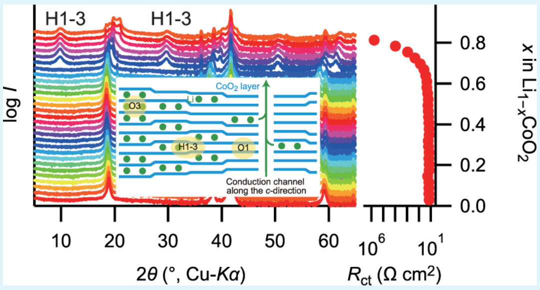

KEYWORDS: *$LiCoO_2$, thin-film battery, epitaxial film, high-voltage charging, phase transition*

1. INTRODUCTION

$LiCoO_2$ is the first cathode material employed in lithium-ion batteries[1,2] and has been used for more than 30 years. Tremendous studies have been done on $LiCoO_2$ during the 30 years and are still in progress in order to realize its potential in practical lithium-ion batteries. For example, although complete lithium deintercalation from $LiCoO_2$ provides a high theoretical capacity of 274 mAh g^{-1}, practical capacity has been limited to ca. 160 mAh g^{-1}. Increasing charge voltage increases the capacity; however, it results in rapid capacity fading. Intensive studies aiming at improving the cycling performance have proposed various mechanisms for the degradation in high-voltage charging: some attribute it to instability of organic electrolytes,[3−5] while others attribute it to structural instability of $LiCoO_2$.

$LiCoO_2$ has O3 structure in which lithium ions reside at its octahedral sites, and the CoO_2 layers are stacked with three-layer periodicity. Lithium deintercalation brings about some phase transitions in $Li_{1-x}CoO_2$. Lithium ions are ordered around $x = 1/2$ to distort the hexagonal crystal lattice to monoclinic.[6] Further lithium deintercalation leads to phase transitions from O3 to H1−3,[7] and then to O1,[8] which change the stacking manner of CoO_2 layers. These phase transitions cause internal stress and subsequent mechanical degradation to $LiCoO_2$ particles, resulting in capacity fading. However, the relation between the phase transitions and cyclability has not been clarified because such phase transitions occurring at high potential are always accompanied by decomposition of the electrolytes. Effects of the phase transitions on the cyclability always overlap that of the electrolyte decomposition, and thus, different values have been reported for the reversible limit of charging voltage.[9−13] Clear relation will be revealed in solid-state systems because side reactions will hardly occur in solid electrolytes.

2. FABRICATION OF THIN-FILM BATTERIES AND IN SITU MEASUREMENTS

This study shows the relation between changes in the crystal structure and electrode properties of $LiCoO_2$ in thin-film solid-state batteries investigated by in situ X-ray diffraction (XRD) combined with electrochemical measurements. Figure 1 schematically illustrates the in situ measurement system and the structure and dimensions of the thin-film battery. The thin-film battery is fabricated on a sapphire *c*-plane. A 9.5 mm square $LiCoO_2$ cathode film is deposited on a sapphire

Received: September 29, 2021
Accepted: November 2, 2021
Published: November 16, 2021

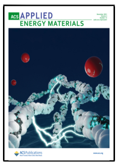

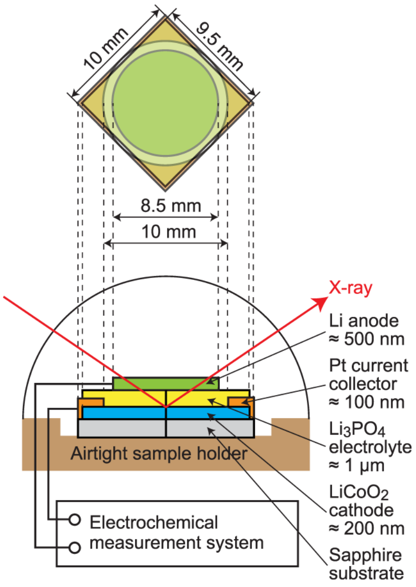

Figure 1. Schematic drawing of the in situ XRD measurement.

substrate kept at 600 °C under an Ar/O_2 atmosphere in which flow rates of Ar and O_2 are 20 and 10 sccm, respectively, by RF magnetron sputtering and then annealed at 700 °C for 5 h in air.

Grain size in the $LiCoO_2$ film is of an order of 100 nm, as shown in the cross-sectional transmission electron microscope (TEM) image in Figure 2a, and the electron diffraction pattern taken from the area covering the $LiCoO_2$ film and sapphire substrate in Figure 2b indicates their epitaxial relation: $LiCoO_2$ is epitaxially grown on the sapphire (0001) plane with the (001) orientation and in-plane alignment of $LiCoO_2$ $[1\bar{1}0]$ ∥ sapphire $[11\bar{2}0]$. On the other hand, the surface scanning electron microscope (SEM) image in Figure 2c shows that the $LiCoO_2$ grains are much larger at the surface. Triangular shape can be recognized in the image, and the grain size is of the order of micrometers, which originates from lateral overgrowth at the end of the deposition.

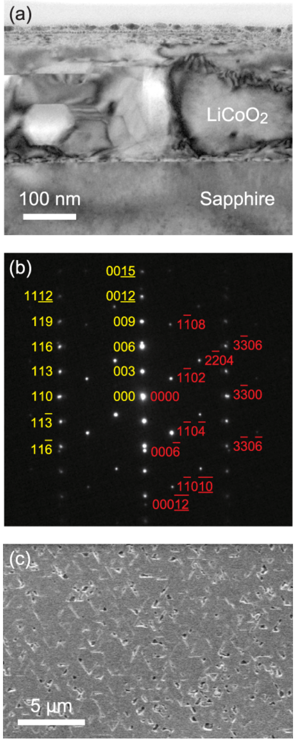

Figure 2. (a) Cross-sectional TEM image, (b) electron diffraction pattern taken along $LiCoO_2$ $[1\bar{1}0]$, and (c) surface SEM image of the $LiCoO_2$ film. The diffraction spots from the $LiCoO_2$ film and sapphire substrate are labeled with Miller indices colored in yellow and red, respectively.

After annealing the $LiCoO_2$ film, Pt is deposited by DC magnetron sputtering as a current collector, which is a square film with 10.0 mm on a side with a circular opening with a diameter of 10 mm. Li_3PO_4 is formed as the solid electrolyte layer with lateral dimensions of 9.5 mm × 9.5 mm by RF magnetron sputtering. Finally, a circular Li anode with a diameter of 8.5 mm is formed above the opening of the Pt current collector by thermal evaporation.

The electrochemical measurement system connected to the battery sealed in an airtight sample holder controls the state-of-charge (SOC) of $LiCoO_2$ and measures electrochemical impedance, while XRD patterns from the thin-film battery are taken in situ in parallel-beam geometry using Cu-Kα radiation. The (001) orientation of the $LiCoO_2$ film is beneficial to detect the phase transitions. The phase transitions accompany clear changes in the *c*-lattice constant, which can be recognized in the basal reflections strengthened by the (001) orientation with high accuracy on the parallel-beam geometry. In addition, the in situ XRD measurement in combination with the electrochemical measurement easily gives structural and electrochemical data at various SOC values to provide detailed relation between the phase transition and electrode properties. Electrochemical impedance spectra are taken in the frequency range from 5×10^5 to 0.1 Hz with an AC amplitude of 20 mV.

3. INFLUENCE OF CHARGING VOLTAGE ON CYCLING PERFORMANCE

Figure 3a shows the charge−discharge curves of the thin-film batteries cycled in the voltage range of 2.5−4.6 V and 2.5−4.2 V in which the thin-film batteries are cycled at a constant current of 11.9 μA. The first discharge capacity is 6.79 μAh, when the thin-film battery is cycled between 2.5 and 4.2 V, while that cycled between 2.5 and 4.6 V is 10.67 μAh; that is, raising the charging cutoff voltage from 4.2 to 4.6 V increases the capacity by 57%; however, it results in the rapid capacity fading: capacity retentions after the 100 cycles are 99% and 79% for the 4.2 and 4.6 V charging, respectively, as shown in Figure 3b. The observed capacity (q) is converted to the specific capacity (Q_{actual}) in the right vertical axis in Figure 3b and SOC (x in $Li_{1-x}CoO_2$) in the left vertical axis in Figure 3c on the basis of the "actual" mass of the $LiCoO_2$ films contributing to the electrode reactions in which the actual mass is estimated as below.

Figure 4a shows the charge−discharge curves in the second cycle obtained from the thin-film batteries cycled in the different voltage ranges. The observed discharge capacity (indicated by q in the uppermost horizontal axis) is 6.79 μAh, when the battery is cycled between 2.5 and 4.2 V, while that cycled between 2.5 and 4.6 V is 10.67 μAh. The apparent specific capacities (Q_{app} in the second horizontal axis) calculated from the observed values (q) and the entire mass of the $LiCoO_2$ films measured using an electric balance (86−87 μg) are only 78 and 123 mAh g^{-1}, respectively, which are much lower than those expected from the relationship between

https://doi.org/10.1021/acsaem.1c03046
ACS Appl. Energy Mater. 2021, 4, 14372−14379

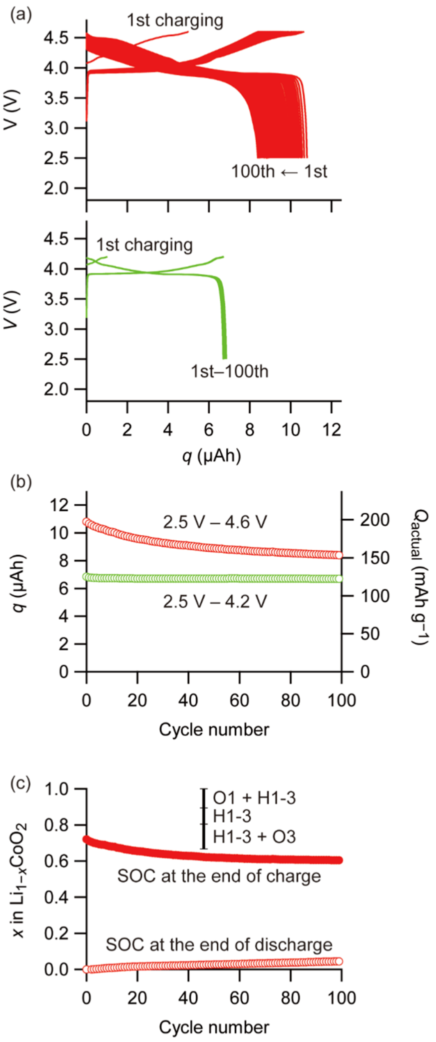

Figure 3. Cycling properties of the thin-film batteries. Charge−discharge curves during the cycling are shown in (a), and changes in the discharge capacities (q) are plotted against the cycle number in (b). The observed capacities in the left vertical axis are converted to specific capacities based on the actual mass for the electrode reactions (Q_{actual}) on the right vertical axis. Changes in SOC values during the cycling between 2.5 and 4.6 V are plotted against the cycle number in (c). Closed and open circles indicate the SOC values at the end of charging and discharging, respectively. The composition range of the H1−3 phase determined by Monte Carlo simulations[20] is also shown by vertical bars.

the charge capacity and the open-circuit voltage of $Li_{1-x}CoO_2$ reported in ref 14: the specific capacities at 4.2 and 4.6 V charging are expected to be 130 and 200 mAh g^{-1}, respectively. The underestimation of the specific capacity comes from the overestimation of active electrode mass.

In the solid-state batteries in this study, the circular Li anode with a diameter of 8.5 mm is formed on the square $LiCoO_2$ cathode with 9.5 mm on a side with a solid electrolyte film of Li_3PO_4 in between, as illustrated in Figure 1. Therefore, only 63% of the cathode faces the Li anode, and it is considered that only this part contributes to the electrode reactions; that is, the actual mass of $LiCoO_2$ for the electrode reactions will be 63% of the measured value. In fact, the specific capacities calculated from the "actual" mass (Q_{actual} in the third horizontal axis) are 124 and 195 mAh g^{-1} for the 4.2 and 4.6 V charging, respectively, which agree with the above expected values. Moreover, transformation to the monoclinic phase that can be recognized in the charge−discharge curves guarantees the validity of the estimation.

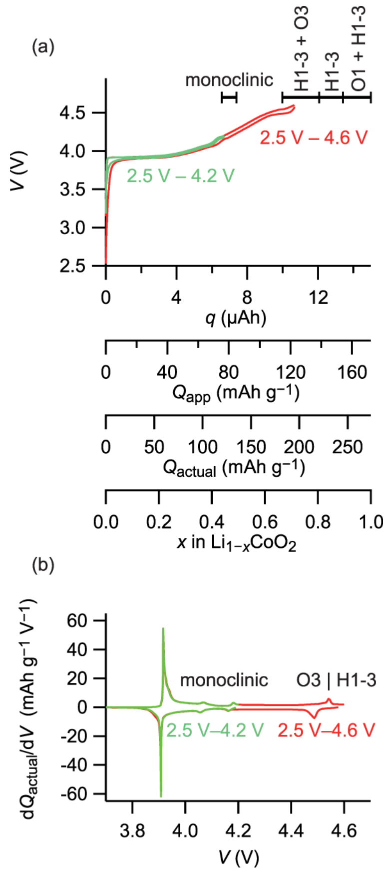

Figure 4. (a) Charge−discharge curves of the thin-film batteries in the second cycle with the charging cutoff voltages of 4.2 and 4.6 V and (b) corresponding differential capacity plots. The vertical axis in (a) indicates the cell voltage, and the horizontal axes indicate observed capacity (q), specific capacity based on the entire mass of the $LiCoO_2$ film (Q_{app}), that based on the actual mass for the electrode reactions (Q_{actual}), and change in the lithium content (x) estimated from the Q_{actual} from the uppermost to the lowermost, respectively. The reported composition ranges for monoclinic,[14] H1−3, and O1 phases[20] are indicated by horizontal bars.

The O3 hexagonal structure of $LiCoO_2$ transforms to monoclinic and returns to the hexagonal phase during charging, and the phase transition appears in the potential profile as small plateaus at ca. 4.1 V between 120 and 135 mAh g^{-1} in the charging capacity[14] and more clearly as a pair of peaks around 4.1 V in the differential capacity (dQ/dV) plot.[6] The differential capacity plots obtained for the present thin-film battery in Figure 4b also have the pair of peaks originating from the phase transition, and the charge−discharge curves in Figure 4a have small plateaus around 4.1 V and Q_{actual} = 120 mAh g^{-1}. That is, transition between hexagonal and monoclinic phases observed in this study falls within the reported composition range of the monoclinic phase, when the specific capacity is calculated from the "actual" mass for the electrode reactions.

The discussion on the "actual" mass of the $LiCoO_2$ film leads to the conclusion that increasing the charging cutoff voltage from 4.2 to 4.6 V increases the specific capacity from 124 to 195 mAh g^{-1} while leading to rapid capacity fading. It should be noted that the first charge capacities are quite different from those in the following cycles, as shown in Figure 3a. In fabrication of thin-film batteries, deposition of solid electrolytes onto cathode layers sometimes changes the lithium contents in the cathodes. For example, deposition of Li_3PO_4 onto $LiNi_{0.5}Mn_{1.5}O_4$ increases its lithium content to convert it to $Li_2Ni_{0.5}Mn_{1.5}O_4$.[15] On the contrary, deposition of Li_3PO_4 onto $LiCoO_2$ in this study decreases the lithium content. We have found that the decrease in the lithium content is controllable by substrate bias in the Li_3PO_4 deposition by RF sputtering, and the details will be reported elsewhere. The differences between the first charge and discharge capacities (Δq) correspond to the amounts of lithium ions extracted in the deposition of Li_3PO_4. Both batteries show the same value of Δq = 5.8 μAh, which are converted to ΔQ_{actual} = 106 mAh g^{-1} and Δx = 0.39, and thus, it is concluded that the Li_3PO_4 deposition partially charges the $LiCoO_2$ to $Li_{0.61}CoO_2$. Therefore, the thin-film batteries must be discharged completely in order to adjust the lithium content to $Li_{1.0}CoO_2$ before investigating the relationship between the electrode properties and crystal phase of $LiCoO_2$ and their dependence on the SOC.

4. RELATION BETWEEN THE ELECTRODE RESISTANCE AND PHASE TRANSITIONS

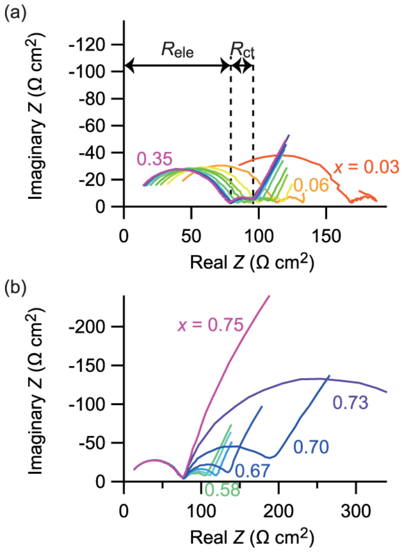

Figure 5. Typical Nyquist plots for the thin-film battery at various SOC values (a) below x = 0.35 and (b) above x = 0.58. The impedance spectra are taken in a frequency range from 5 × 10^5 to 0.1 Hz with an AC amplitude of 20 mV.

Figure 5 shows typical Nyquist plots obtained for the thin-film battery obtained at various SOC values. The Nyquist plots consist of two semicircles and a straight line. The diameter of the semicircles in the higher frequencies is independent of the SOC and agrees with that estimated from the conductivity and dimensions of the Li_3PO_4 film, and thus, it is attributable to the resistance of the electrolyte layer (R_{ele}). The battery shows a little higher resistance at shallow SOC values, e.g., at x = 0.03, as indicated in Figure 5a. It is because the cathode in this battery has a current collector only on its edge, and $LiCoO_2$ is a semiconductor. Because it is resistive before lithium deintercalation provides metallic conduction,[16] the battery shows somewhat high resistance at shallow SOC values. The second semicircle shows SOC dependence, indicating that it is attributable to the charge-transfer resistance at the cathode (R_{ct}). R_{ct} observed in Figure 5a is ca. 14 Ω cm^2, which is comparable to that observed for a (001)-oriented $LiCoO_2$/Lipon interface.[17] On the other hand, R_{ct} noticeably starts to increase at x = 0.67 and reaches 5.6 × 10^5 Ω cm^2 at x = 0.81, as shown in Figures 5b and 6.

Oxidative decomposition of electrolytes caused by high-voltage charging generally increases R_{ct} in liquid electrolyte systems;[5] however, the increase in R_{ct} in this battery will not come from decomposition of Li_3PO_4. First-principles calculations show that the oxidation potential of Li_3PO_4 is 4.2 V vs Li^+/Li,[18] whereas some experimental results suggest that its practical electrochemical window is much wider than the thermodynamic value due to slow kinetics of the decomposition reactions. In fact, experimental results indicate that Li_3PO_4 and a related material, Lipon, are stable against a 5 V cathode, $LiNi_{0.5}Mn_{1.5}O_4$. Interfacial resistance between $LiNi_{0.5}Mn_{1.5}O_4$ and Li_3PO_4 is as low as 7.6 Ω cm^2, and a Li/Li_3PO_4/$LiNi_{0.5}Mn_{1.5}O_4$ battery shows stable cycling even at an elevated temperature of 70 °C.[15] In addition, a Li/Lipon/$LiNi_{0.5}Mn_{1.5}O_4$ battery delivers a remarkable capacity retention of 90% over 10,000 cycles with coulombic efficiency higher than 99.98%.[19] These results strongly suggest that Li_3PO_4 is not oxidatively decomposed at 4.7 V vs Li^+/Li, which is the electrode potential of $LiNi_{0.5}Mn_{1.5}O_4$ in its charged state, to increase the electrode resistance. On the other hand, R_{ct} in this thin-film battery starts to increase at x = 0.67 obviously, even though the cathode potential is still 4.55 V there. The reason for the different stability against high-voltage charging from the above studies will be found in the differences in the cathodes, for instance, in the crystal structure. $LiCoO_2$ has a two-dimensional layered structure, while $LiNi_{0.5}Mn_{1.5}O_4$ has a three-dimensional spinel structure.

Figure 6 shows the XRD patterns obtained at various SOC values along with R_{ct} values derived from the Nyquist plots in Figure 5. The XRD pattern before charging consists of basal reflections from $LiCoO_2$ indicating the (001) orientation of the film, 110 and 200 reflections from the Li metal anode, and 0003 and 0009 reflections from the sapphire substrate, where forbidden sapphire 0003 reflection appears due to the epitaxial strain. The basal reflections shift to the lower angles upon charging, which indicates expansion of the c axis caused by the weakening coulombic attraction between CoO_2 and Li layers with the lithium deintercalation. When the SOC comes to x = 0.67, a new series of diffractions emerges at 2θ = 9.7, 19.5, 29.7, 39.7, 50.5, and 61.3 °, which are assignable to 003$\underline{n}$ (n = 1−6) reflections of the H1−3 phase.[20] Further lithium deintercalation gives a rise of new reflections at 2θ = 20.96 and 41.78 °, which are 001 and 002 reflections from the O1 phase, i.e., lithium-depleted CoO_2.[21] The right panel of Figure 6 shows SOC dependence of R_{ct} taken with the XRD patterns. The R_{ct} is almost unchanged before the emergence of the H1−3 phase and then starts to increase. The coincidence of onset of increasing R_{ct} and emergence of the H1−3 phase strongly suggests that the formation of the H1−3 phase increases the R_{ct}.

The H1−3 phase is a second stage structure in $Li_{1-x}CoO_2$, which is composed of CoO_2 layers piled up with two kinds of interlayers alternately: one is O3-type with an interlayer distance of 4.8 Å, and the other is O1-type with an interlayer distance of 4.2 Å, as illustrated in Figure 7a.[7] A kinetic Monte Carlo simulation has revealed that the chemical diffusion

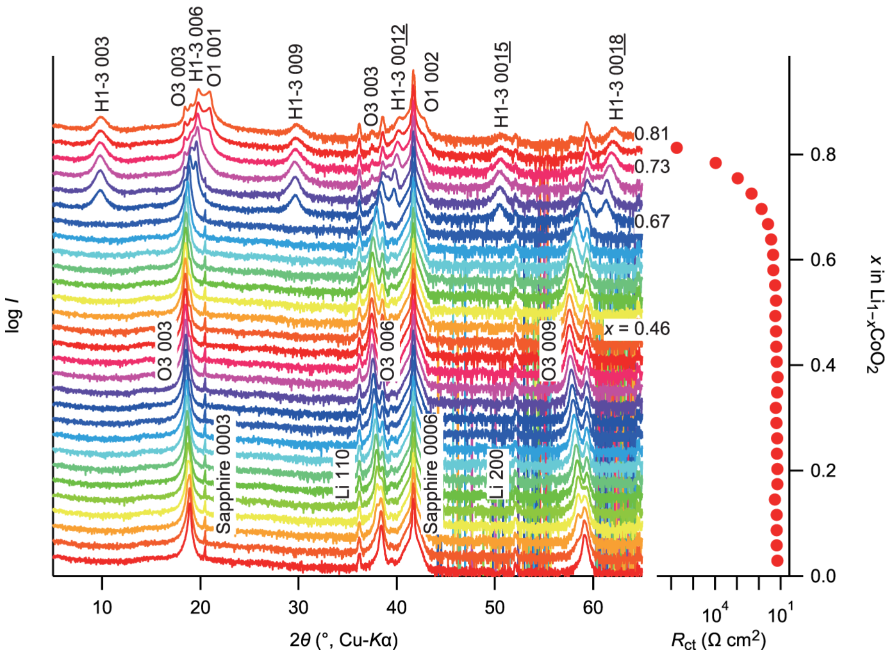

Figure 6. XRD patterns and R_{ct} measured for the thin-film battery during charging. Diffraction intensity (I) and R_{ct} are plotted on the logarithmic scales. Some XRD patterns referred in the text are labeled with the SOC values.

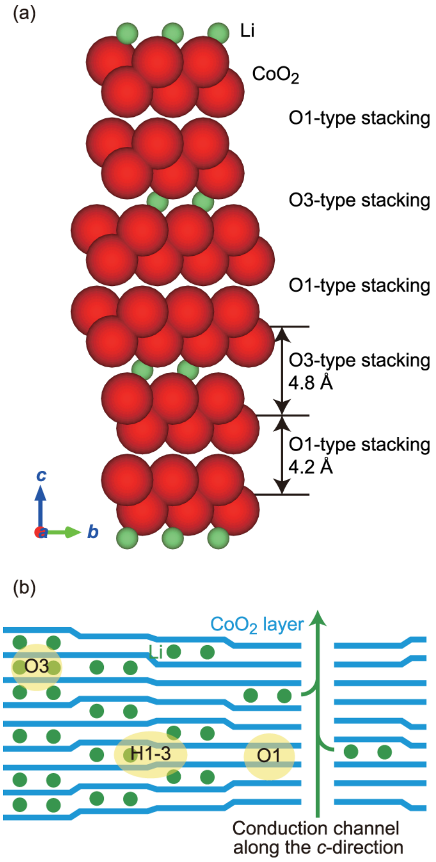

Figure 7. (a) Crystal structure of the H1−3 phase[7] and (b) schematic representation of lithium deintercalation from the (001)-oriented $LiCoO_2$ film. Crystal structure is presented in a space-filling structure model drawn by VESTA.[34]

coefficient in $Li_{1-x}CoO_2$ decreases by five orders of magnitude beyond $x = 0.6$ due to the high activation barrier for Li^+-ionic diffusion.[22] The high activation barrier is attributed to two factors. One is a drop of the c-lattice constant, which compresses the tetrahedral sites along the conduction paths. The second factor is increasing effective charge on the Co ion that exerts a large electrostatic repulsion to the Li^+ ion in the tetrahedral sites. Because the effective charge on the Co ion will increase gradually during charging, the drastic increase of R_{ct} with the emergence of the H1−3 phase implies that the former is the predominant factor in this case; that is, the drop of the interlayer distance to 4.2 Å makes the gallery height insufficient for fast ionic diffusion.

The $LiCoO_2$ film grown on the sapphire c-plane has the (001) orientation in which the interlayers are parallel to the substrate and perpendicular to the current direction. Although lithium ions are considered to hardly diffuse along the c direction, (001)-oriented films have been reported to show smooth charge−discharge reactions.[23−25] It is deduced that lithium ions can diffuse along the c direction through defects, e.g., grain boundaries, antiphase boundaries, and pairs of antisite Li and oxygen vacancies acting as the conduction channels. Figure 7b schematically presents lithium extraction from (001)-oriented $LiCoO_2$. Lithium extraction to $x \approx 0.65$ in $Li_{1-x}CoO_2$ is reported to expand the interlayer spacing from 4.7 to 4.8 Å, maintaining its O3 structure.[14] Further extraction depletes lithium ions in the alternate interlayers to decrease their height to 4.2 Å and form the H1−3 phase, and complete extraction of lithium ions leads to the formation of the O1 phase in which all the CoO_2 layers are piled up with an interlayer distance of 4.2 Å. Since the charge reaction will preferentially extract lithium ions neighboring to the "conduction channel along the c direction," 4.2-Å-high galleries will be formed to surround the "channel" and impede the supply of lithium ions to the "channel." In addition, lithium ions must undergo long lateral diffusion to reach the "channel" in the present epitaxial film, as indicated in Figure 2c. Therefore, lithium ions around the "channel" will be depleted to make the channel inactive and increase R_{ct} right after the emergence of the H1−3 phase. The XRD patterns on the top

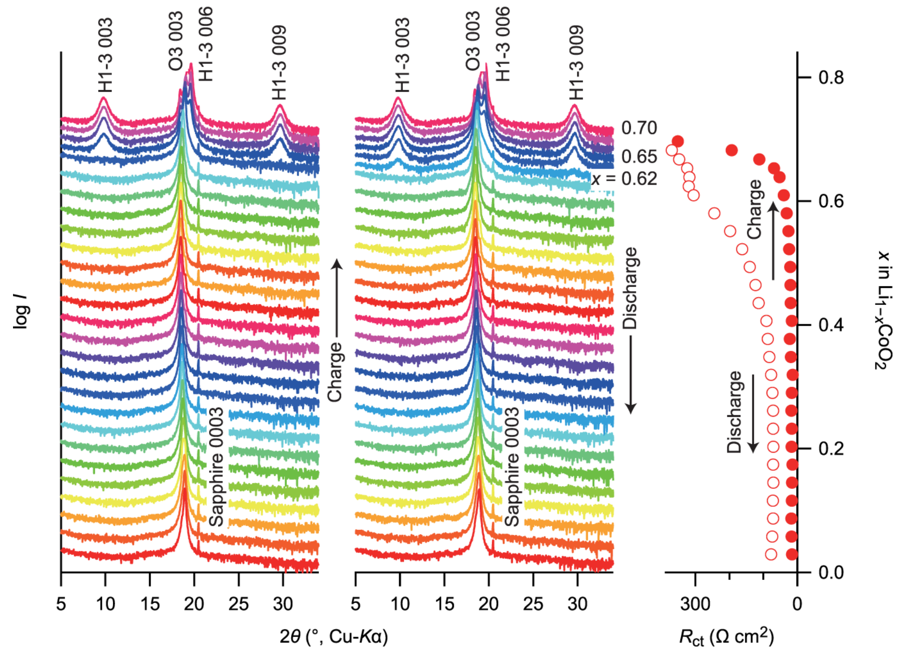

Figure 8. XRD patterns and R_{ct} measured for the thin-film battery during the charging up to x = 0.7 and discharging. Diffraction intensity (I) is plotted on the logarithmic scales. Some XRD patterns referred in the text are labeled with the SOC values. Closed and open circles in the right panel indicate R_{ct} in the charging and discharging process, respectively.

in Figure 6 support this scheme. They consist of three basal reflection series, indicating the coexistence of O3, H1−3, and O1 phases, although the H1−3 phase should coexist only with either the O3 or O1 phase thermodynamically.[26,27] Despite the thermodynamic instability, the three-phase coexistence will be allowed due to the slow kinetics. The 4.2 Å galleries will impede the movement of lithium ions from O3 to H1−3 and O1 phases that vanishes the O3 phase.

5. EFFECTS OF PHASE TRANSITIONS ON THE CYCLING PERFORMANCE

Lithium reintercalation recovers the original O3 structure, as shown in Figure 8; however, the recovery is somewhat sluggish. In Figure 8, $Li_{1-x}CoO_2$ is charged up to x = 0.70 and then discharged. Reflections from the H1−3 phase appear at x = 0.65 in the charging while surviving until x = 0.62 in the discharging. In addition, R_{ct} shown in the right panel starts to increase rapidly at x = 0.65 in the charging while decreasing during the discharging slowly. The sluggish recovery will be due to the slow kinetics: lithium ions must prop up the galleries from 4.2 to 4.8 Å in height in order to recover the O3 phase. In fact, the decreasing R_{ct} value is accelerated to some extent after the H1−3 phase disappears. However, the R_{ct} does not go back to its original value: The R_{ct} is 16 Ω cm^2 before the charging, while it is ca. 70 Ω cm^2 at the end of discharging.

The irreversible increase in R_{ct} should be the reason for the rapid capacity fading observed in the cycling with 4.6 V charging because the charge−discharge curves overlap the composition range for the H1−3 phase determined by Monte Carlo simulations[20] at the end of charging to 4.6 V, as shown in Figure 4a. In fact, the formation of the H1−3 phase appears as a potential plateau in Figure 4a, which gives a peak around 4.6 V in the corresponding differential capacity plot in Figure 4b, and diffractions from the H1−3 phase are detected in the XRD patterns in Figures 6 and 8. The irreversible increase in R_{ct} will be caused by the large change in the gallery height in the transformation between the O3 and H1−3 phases. The difference in the interlayer distance between O3 and O1-type exceeds 10%. In addition, the transformation between O3 and O1-type galleries accompanies lateral shift of the CoO_2 layers. Such structure changes will degrade the $LiCoO_2$ film to increase the resistance and lead to the capacity fading in the cycling with high-voltage charging. On the other hand, the cycling between 2.5 and 4.2 V is very stable because it changes the SOC between x = 0 and 0.46, where the O3 structure is kept, and the corresponding change in the interlayer distance is between 4.68 and 4.80 Å, i.e., only 2%.

Phase transitions taking place in high-voltage charging have been considered to affect the cycling performance of $LiCoO_2$; however, their direct relation has not been clarified because high-voltage charging also brings about side reactions that veil the direct relation, e.g., formation of resistive LiF films on the surface,[28] pitting corrosion,[29] or dissolution of Co.[30] Such side reactions make the relation between the phase transitions and cycling performance unclear, and an increase in electrode impedance has been always attributed to the electrode/electrolyte interface.[31,32] On the other hand, Li_3PO_4 used as the solid electrolyte in this study has unveiled the relation between the phase transition and electrode properties because it suppresses the side reactions and provides stable and low-resistive interface even to $LiNi_{0.5}Mn_{1.5}O_4$ that shows an electrode potential of 4.7 V.[15,19]

The high-voltage cycling properties of $LiCoO_2$ have been generally investigated in liquid electrolytes, whereas they were once reported for an Li/Lipon/$LiCoO_2$ thin-film battery.[33] The battery in the paper shows very stable cycling below 4.4 V, while increasing the cutoff voltage higher than 4.4 V results in capacity fading and an increase in the cell resistance. This study provides detailed explanations of the results. The phase transition leading to the degradation of the battery will be that between O3 and H1−3, although it was assigned to that between O3 and O1 in the paper because it takes place just above 4.5 V, where the H1−3 phase is detected in this study. The thin-film battery cycled with an upper cutoff voltage of 5.0 V in the paper shows quicker capacity fading than that with 4.6 V in this study, which is due to the different cutoff voltages. The SOC values at the end of charging and discharging in this study are estimated from the accumulated capacity and plotted in Figure 3c. The SOC values at the end of charging become shallower upon the cycling because increasing R_{ct} enlarges the overpotential. The increased overpotential makes $LiCoO_2$ never reach the composition for the O3/H1−3 phase transition and thus lowers the degradation rate in the prolonged cycle.

6. CONCLUSIONS

This study has revealed the clear relation between electrode kinetics and phase transition in high-voltage charging of $LiCoO_2$. Combination of impedance spectroscopy and in situ XRD shows that a drastic increase in electrode resistance coincides with phase transition from O3 to H1−3 phases. The coincidence strongly suggests that O1-type interlayers with a gallery height of 4.2 Å formed in the H1−3 phase impede ionic diffusion to reduce the electrode kinetics of $LiCoO_2$ charged at high voltage. Once $LiCoO_2$ has experienced the phase transition, the increased electrode resistance never comes back to its original value in the following discharging even though it recovers its O3 phase. It will be the large difference in the interlayer distance between the O3 and O1-type galleries, which leads to the irreversible increase in the electrode resistance and capacity fading.

AUTHOR INFORMATION

Corresponding Author

Kazunori Takada − *Center for Green Research on Energy and Environmental Science, National Institute for Materials Science, Tsukuba, Ibaraki 305-0044, Japan;* orcid.org/0000-0001-7568-1806; Phone: +81 29 8604317; Email: takada.kazunori@nims.go.jp

Authors

Tsuyoshi Ohnishi − *Center for Green Research on Energy and Environmental Science, National Institute for Materials Science, Tsukuba, Ibaraki 305-0044, Japan;* orcid.org/0000-0002-2333-7752

Kazutaka Mitsuishi − *Research Center for Advanced Measurement and Characterization, National Institute for Materials Science, Tsukuba, Ibaraki 305-0047, Japan;* orcid.org/0000-0002-9361-4057

Complete contact information is available at:
https://pubs.acs.org/10.1021/acsaem.1c03046

Author Contributions

The manuscript was written through contributions of all authors. All authors have given approval to the final version of the manuscript.

Notes

The authors declare no competing financial interest.

ACKNOWLEDGMENTS

This work was partly supported by the Advanced Low Carbon Technology Research and Development Program, Specially Promoted Research for Innovative Next Generation Batteries (ALCA-SPRING) of the Japan Science and Technology Agency (JST), Japan; a Materials Processing Science project ("Materealize") of Ministry of Education, Culture, Sports, Science and Technology, Japan (MEXT); a KAKENHI Grant-in-Aid for Scientific Research on Innovative Areas "Interface IONICS" (grant number JP19H05813) from the Japan Society for the Promotion of Science (JSPS); and JST grant number JPMJPF2016. We thank Rigaku Corporation for letting us to use the air-tight sample holder.

REFERENCES

(1) Mizushima, K.; Jones, P. C.; Wiseman, P. J.; Goodenough, J. B. Li_xCoO_2 ($0<x\leq1$): a new cathode material for batteries of high energy density. *Mater. Res. Bull.* **1980**, *15*, 783−789.

(2) Yoshino, A. The birth of the lithium-ion battery. *Angew. Chem., Int. Ed.* **2012**, *51*, 5798−5800.

(3) Hu, S. K.; Cheng, G. H.; Cheng, M. Y.; Hwang, B. J.; Santhanam, R. Cycle life improvement of ZrO_2-coated spherical $LiNi_{1/3}Co_{1/3}Mn_{1/3}O_2$ cathode material for lithium ion batteries. *J. Power Sources* **2009**, *188*, 564−569.

(4) Zuo, X. X.; Fan, C. J.; Liu, J. S.; Xiao, X.; Wu, J. H.; Nan, J. M. Effect of tris(trimethylsilyl)borate on the high voltage capacity retention of $LiNi_{0.5}Co_{0.2}Mn_{0.3}O_2$/graphite cells. *J. Power Sources* **2013**, *229*, 308−312.

(5) Wu, S. P.; Lin, Y. L.; Xing, L. D.; Sun, G. Z.; Zhou, H. B.; Xu, K.; Fan, W. Z.; Yu, L.; Li, W. S. Stabilizing $LiCoO_2$/graphite at high voltages with an electrolyte Additive. *ACS Appl. Mater. Interfaces* **2019**, *11*, 36244−36251.

(6) Reimers, J. N.; Dahn, J. R. Electrochemical and in situ X-ray diffraction studies of lithium intercalation in Li_xCoO_2. *J. Electrochem. Soc.* **1992**, *139*, 2091−2097.

(7) Chen, Z.; Lu, Z.; Dahn, J. R. Staging phase transitions in Li_xCoO_2. *J. Electrochem. Soc.* **2002**, *149*, A1604−A1609.

(8) Amatucci, G. G.; Tarascon, J. M.; Klein, L. C. CoO_2, the end member of the Li_xCoO_2 solid solution. *J. Electrochem. Soc.* **1996**, *143*, 1114−1123.

(9) Amatucci, G. G.; Tarascon, J. M.; Klein, L. C. Cobalt dissolution in $LiCoO_2$-based non-aqueous rechargeable batteries. *Solid State Ionics* **1996**, *83*, 167−173.

(10) Wang, H.; Jang, Y. I.; Huang, B.; Sadoway, D. R.; Chiang, Y. M. TEM study of electrochemical cycling-induced damage and disorder in $LiCoO_2$ cathodes for rechargeable batteries. *J. Electrochem. Soc.* **1999**, *146*, 473−480.

(11) Chen, Z.; Lu, Z.; Cho, J.; Kim, Y. J.; Kim, T. J.; Park, B. Zero-strain intercalation cathode for rechargeable Li-ion cell. *Angew. Chem., Int. Ed.* **2001**, *40*, 3367−3369.

(12) Chen, Z.; Dahn, J. R. Methods to obtain excellent capacity retention in $LiCoO_2$ cycled to 4.5 V. *Electrochim. Acta* **2004**, *49*, 1079−1090.

(13) Xia, H.; Lu, L.; Meng, Y. S.; Ceder, G. Phase transitions and high-voltage electrochemical behavior of $LiCoO_2$ thin films grown by pulsed laser deposition. *J. Electrochem. Soc.* **2007**, *154*, A337−A342.

(14) Ohzuku, T.; Ueda, A. Solid-state redox reactions of $LiCoO_2$ ($R\bar{3}m$) for 4 volt secondary lithium cells. *J. Electrochem. Soc.* **1994**, *141*, 2972−2977.

(15) Kawasono, H.; Shiraki, S.; Suzuki, T.; Shimizu, R.; Hitosugi, T. Extremely low resistance of Li_3PO_4 electrolyte/$Li(Ni_{0.5}Mn_{1.5})O_4$ electrode interfaces. *ACS Appl. Mater. Interfaces* **2018**, *10*, 27498−27502.

(16) Milewska, A.; Swierczek, K.; Tobola, J.; Boudoire, F.; Hu, Y.; Bora, D. K.; Mun, B. S.; Braun, A.; Molenda, J. The nature of the nonmetal−metal transition in Li_xCoO_2 oxide. *Solid State Ionics* **2014**, *263*, 110−118.

(17) Haruta, M.; Shiraki, S.; Suzuki, T.; Kumatani, A.; Ohsawa, T.; Takagi, Y.; Shimizu, R.; Hitosugi, T. Negligible "negative space-charge layer effects" at oxide-electrolyte/electrode interfaces of thin-film batteries. *Nano Lett.* **2015**, *15*, 1498−1502.

(18) Zhu, Y.; He, X.; Mo, Y. Origin of outstanding stability in the lithium solid electrolyte materials: Insights from thermodynamic

analyses based on first-principles calculation. *ACS Appl. Mater. Interfaces* **2015**, *7*, 23685−23693.

(19) Li, J. C.; Ma, C.; Chi, M. F.; Liang, C. D.; Dudney, N. J. Solid electrolyte; the key for high-voltage lithium batteries. *Adv. Energy Mater.* **2015**, *5*, No. 1401408.

(20) Van der Ven, A.; Aydinol, M. K.; Ceder, G.; Kresse, G.; Hafner, J. First-principles investigation of phase stability in Li_xCoO_2. *Phys. Rev. B* **1998**, *58*, 2975−2987.

(21) Tarascon, J. M.; Vaughan, G.; Chabre, Y.; Seguin, L.; Anne, M.; Strobel, P.; Amatucci, G. In-situ structural and electrochemical study of $Ni_{1-x}Co_xO_2$ metastable oxides prepared by soft chemistry. *J. Solid State Chem.* **1999**, *147*, 410−420.

(22) Van der Ven, A.; Ceder, G. Lithium diffusion in Layered Li_xCoO_2. *Electrochem. Solid-State Lett.* **2000**, *3*, 301−304.

(23) Shiraki, S.; Shirasawa, T.; Suzuki, T.; Kawasoko, H.; Shimizu, R.; Hitosugi, T. Atomically well-ordered structure at solid electrolyte and electrode interface reduces the interfacial resistance. *ACS Appl. Mater. Interfaces* **2018**, *10*, 41732−41737.

(24) Kawashima, K.; Ohnishi, T.; Takada, K. High-rate capability of $LiCoO_2$ cathodes. *ACS Appl. Energy Mater.* **2020**, *3*, 11803−11810.

(25) Hasegawa, G.; Kuwata, N.; Tanaka, Y.; Miyazaki, T.; Ishigaki, N.; Takada, K.; Kawamura, J. Tracer diffusion coefficients of Li^+ ions in *c*-axis oriented Li_xCoO_2 thin films measured by secondary ion mass spectrometry. *Phys. Chem. Chem. Phys.* **2021**, *23*, 2438−2448.

(26) Abe, T.; Koyama, T. Thermodynamic modeling of the $LiCoO_2-CoO_2$ pseudo-binary system. *Calphad* **2011**, *35*, 209−218.

(27) Chang, K.; Hallstedt, B.; Music, D.; Fischer, J.; Ziebert, C.; Ulrich, S.; Seifert, H. J. Thermodynamic description of the layered O3 and O2 structural $LiCoO_2-CoO_2$ pseudo binary systems. *Calphad* **2013**, *41*, 6−15.

(28) Sun, Y.-K.; Han, J.-M.; Myung, S.-T.; Lee, S.-W.; Amine, K. Significant improvement of high voltage cycling behavior AlF_3-coated $LiCoO_2$ cathode. *Electrochem. Commun.* **2006**, *8*, 821−826.

(29) Yano, A.; Shikano, M.; Ueda, A.; Sakaebe, H.; Ogumi, Z. $LiCoO_2$ degradation behavior in the high-voltage phase transition region and improved reversibility with surface coating. *J. Electrochem. Soc.* **2017**, *164*, A6116−A6122.

(30) Hirooka, M.; Sekiya, T.; Omomo, Y.; Yamada, M.; Katayama, H.; Okumura, T.; Yamada, Y.; Ariyoshi, K. Degradation mechanism of $LiCoO_2$ under float charge conditions and high temperatures. *Electrochim. Acta* **2019**, *320*, No. 134596.

(31) Aurbach, D.; Markovsky, B.; Rodkin, A.; Levi, E.; Cohen, Y. S.; Kim, H.-J.; Schmidt, M. On the capacity fading of $LiCoO_2$ intercalation electrodes: the effect of cycling, storage, temperature, and surface film forming additives. *Electrochim. Acta* **2002**, *47*, 4291−4306.

(32) Andersson, A. M.; Abraham, D. P.; Haasch, R.; MacLaren, S.; Liu, J.; Amine, K. Surface characterization of electrodes from high power lithium-ion batteries. *J. Electrochem. Soc.* **2002**, *149*, A1358−A1369.

(33) Jang, Y.-I.; Dudney, N. J.; Blom, D. A.; Allard, L. F. Electrochemical and electron microscopic characterization of thin-film $LiCoO_2$ cathodes under high-voltage cycling conditions. *J. Power Sources* **2003**, *119−121*, 295−299.

(34) Momma, K.; Izumi, F. VESTA 3 for three-dimensional visualization of crystal, volumetric and morphology data. *J. Appl. Crystallogr.* **2011**, *44*, 1272−1276.